J Solid State Electrochem (2012) 16:3443–3448
DOI 10.1007/s10008-012-1841-1

ORIGINAL PAPER

# Ultrafast anode for high voltage aqueous Li-ion batteries

**M. D. Levi · Yu. Shilina · G. Salitra · D. Aurbach · E. Guyot · S. Seghir · J. M. Lecuire · C. Boulanger**

Received: 3 July 2012 / Revised: 1 August 2012 / Accepted: 3 August 2012 / Published online: 15 August 2012


**Abstract** Clustered Mo sulfide $Mo_6S_8$ (Chevrel phase) demonstrates outstandingly high rate capability in contact with concentrated aqueous $Li_2SO_4$ solutions. Slow galvanostatic cycling can be performed with good Faradaic efficiency at a moderate capacity of 32.1 $mAhg^{-1}$ ($1e^-$ reduction of $Mo_6S_8$), which in combination with $1e^-$ oxidation process in $Li_xMn_2O_4$ cathode, results in equilibrium cell voltage of 1.5 V. Higher rates of charge and discharge have been also achieved within a considerably extended apparent electrochemical stability window involving second two-electron reduction of $Mo_6S_8$ which leads to apparent cell voltage of 1.85 V, specific capacity about 74.7 $mAhg^{-1}$ at 90 % Faradaic efficiency, specific energy of 74 $Whkg^{-1}$ (related to both electrodes) at extremely high charge–discharge rate of 60 C. Our study highlights the generic feature of Li-ion aqueous cells, namely, a high rate capability coupled with a relatively fast self-discharge which necessitates a more profound understanding of the nature of self-discharge in Li-ion insertion hosts in contact with aqueous solutions.

**Keywords** Aqueous Li-ion batteries · Ultrafast anode · Chevrel phase · High rate capability · $Li_xMn_2O_4$ spinel cathode · Self-discharge

This study is dedicated to Prof. W. Plieath's 75th birthday.

M. D. Levi (✉) · Y. Shilina · G. Salitra · D. Aurbach
Department of Chemistry, Bar-Ilan University,
Ramat Gan 52900, Israel
e-mail: levimi@mail.biu.ac.il

E. Guyot · S. Seghir · J. M. Lecuire · C. Boulanger
Université de Lorraine, CNRS, Institut Jean Lamour,
Electrochemistry of Materials,
UMR 7198,
57078 Metz Cedex 1, France

## Introduction

Commercial Ni–Cd, Ni–MH (metal hydride), and $Pb/PbO_2$ rechargeable batteries operating with aqueous alkaline and acidic solutions, respectively, suffer from low operating voltage due to the limited electrochemical stability window (ESW) of aqueous solutions (1.23 V under conditions close to equilibrium). Li-ion battery technology commercialized in early 1990s deals with aprotic electrolyte solutions with the characteristic ESW much wider compared to that for the suitable aqueous solutions. The charge–discharge voltages of 3, 4, or even 5 V can be easily reached with Li-ion insertion hosts in aprotic solutions; the latter usually in the presence of special organic additives or ionic liquids [1]. Despite the fact that conventional Li-ion batteries successfully conquer new markets of small- and middle-scale battery applications (e.g., portable electronics and electric vehicles), serious drawbacks such as safety hazards due to electrodes overcharging and thermal abuse, high toxicity and flammability of many organic solvents used, high costs of batteries components, etc. should not be ignored. Li-ion batteries employing aqueous solutions could become an efficient alternative to conventional Li-ion cells. Dahn et al. [2–4] reported that Li-ions insertion–deinsertion into several types of intercalation hosts may readily proceed in aqueous solutions with a reasonably high Faradaic efficiency (FE). However, despite a continuously growing number of recent publications on this topic, [5–7] the mechanisms of Li-ion insertion reactions in aqueous Li-ion batteries (AqLiB) are not understood in full detail. The choice of the suitable intercalation hosts, a non-trivial link between the width of the ESW and solution composition [8], and, finally, coupling between a typically high rate capability and the relatively fast self-discharge rate of the electrodes are the major problems requiring novel solutions.

Here, we report that clustered Mo sulfide ($Mo_6S_8$ often also called Chevrel phase) previously known as an intercalation

host accommodating highly mobile $Li^+$ and $Mg^{2+}$ ions [9] and multivalent cations [10, 11] from various organic solvents, used also as an effective electrochemical junction unit (a solid-state membrane) for separation of different cations in aqueous solutions [12, 13], is shown to be a unique ultrafast anode for AqLiB. $1e^-$ reduction process of $Mo_6S_8$ results in a moderate specific capacity of 32.1 $mAhg^{-1}$ and equilibrium voltage of 1.5 V with $Li_xMn_2O_4$ cathode results in equilibrium charge–discharge voltage of 1.5 V. A sufficiently higher apparent cell voltage of 1.85 V with specific capacity about 74.7 $mAhg^{-1}$ at 90 % FE and specific energy of 74 $Whkg^{-1}$ (related to both electrodes) can be achieved at an extraordinary high rate of charge and discharge of 60 C at the expense of increased self-discharge at lower charging–discharging rates.

## Experimental part

$LiMn_2O_4$ compound was synthesized by reaction of stoichiometric mixtures of $Li_2CO_3$ and $MnCO_3$ (Sigma-Aldrich). The mixture of analytical grade precursors (>99.9 %) was calcined for 8 h at 800 °C for $LiMn_2O_4$ to yield the desired oxide powders. According to a procedure earlier reported [11], $Cu_3Mo_6S_8$ powder was obtained by the solid state reaction (1,000 °C, 50 h) of a well-homogenized stoichiometric mixture of Cu, $MoS_2$, and Mo fine powder. The de-intercalation of copper of $Cu_3Mo_6S_8$ was carried out chemically (HCl 6 M) or electrochemically (at 0.400 V/SCE for 420 min) and led to $Mo_6S_8$ XRD controls which evidenced that the powders are free of secondary phase ($MnO_2$ or $LiMnO_2$ for $Li_2Mn_2O_4$ and $MoS_2$ for $Mo_6S_8$). The sizes of the more or less circular grains, determined by SEM examinations, are ranging from 0.4 to 0.8 μm for $Li_2Mn_2O_4$ and from 2 to 5 μm for $Mo_6S_8$.

The electrodes were fabricated from a mixture of active materials ($Mo_6S_8$ or $Li_xMn_2O_4$), SuperP conductive carbon black, and the PVdF binder in a ratio (by weight) of 8:1:1 pressed onto a stainless steel grid. The electrodes were punched in the form of disks with a typical diameter of 4–5 mm. The mass load of the active material was between 2 and 4 mg. The electrodes were dried at 120 °C overnight before assembly. $Li_2SO_4$ (2 M) prepared using doubly distilled water served as the electrolyte solution. Two types of electrochemical cells were employed: (a) a flooded three-electrode cell purged from air by flow of pure Ar and (b) a semi-starved Hohsen-type cells with glassy paper separator. For the characterization of $Mo_6S_8$ anode and $Li_xMn_2O_4$ cathode, the high surface area-activated carbon cloth K2000 was used as the counter-electrode. In flooded cells, saturated (sat.) Ag/AgCl was used as the reference electrode (the potential's stability, determined from the value of the middle-peak potential of the cyclic voltammogram (CV) curve measured at the same scan rate, was in the range of ±1 mV), whereas in the Hohsen cell, in view of the lack of space for a true reference electrode, a piece of K2000 was used as the quasi-reference electrodes with further re-calculation of the measured potentials with respect to sat. Ag/AgCl. Autolab-30 controlled by GPES software was used for the CV and galvanostatic measurements.

## Results and discussion

Figure 1a shows the CVs of $Mo_6S_8$ electrode in the form of the differential capacity, i.e., dividing the CV current by the scan rate. It is seen that electroreduction of $Mo_6S_8$ is a highly reversible process with formal redox potential around −0.75 V; however, at the potentials lower than −0.8 V, an increase in the cathodic current becomes essential as the scan rate decreases. The following galvanostatic test was used to identify the stoichiometry of the resulting $Li_xMo_6S_8$ when charged down to −1.17 V (Fig. 1b). It is seen that the first redox potential of $Mo_6S_8$ at −0.75 V relates to $1e^-$ reduction, whereas the second reduction plateau (redox potential near −1.1 V), at a current of 1 mA applied for the different periods of time, results in only 10 % increase in the discharge capacity at the expense of a dramatic decrease of the FE of the entire reduction process (the right black curve in Fig. 1b).

Attempts to maximize the extent of reversible Li-ion insertion with good FE were carried out under different applied currents along first $1e^-$ reduction plateau (with the cut-off potential higher than −1.0 V). The results shown in Fig. 1c for the current values ranging from 0.1 to 2 mA together with the calculated percent of the depth of $Mo_6S_8$ charge (expressed by the number of $e^-$ per $Mo_6S_8$ unit) and the related FE (see inset in this figure) demonstrate clearly that this electrode is incredibly fast with respect to Li-ion insertion–deinsertion in aqueous solutions. $Mo_6S_8$ is thus the ultrafast anode with most negative redox potential in aqueous solutions, very close to the end of the ESW limited by the electroreduction of water molecules. We reached the capacity related to the transfer of $1e^-$ per $Mo_6S_8$ unit with the FE of 0.85, 0.88, and 0.98 at 1.37, 13.7, and 25.4 C rate, respectively. The voltage profiles for both charge and discharge are extremely flat.

Similar combined CV and galvanostatic tests were performed with $Li_xMn_2O_4$ electrode (subpanels a, b, and c, respectively, of Fig. 2). It is seen that at the potentials higher than 0.8 V, a parasitic anodic process, most probably, due to electrooxidation of water, interferes with the formation of a strongly delithiated form of $Li_xMn_2O_4$ (confirmed also by a considerable current increase at 60 °C, see panel b). The involvement of parasitic reactions close to the potential of formation of the diluted (in Li content) $Li_xMn_2O_4$ is not as strong as that for the heavily lithiated form of $Mo_6S_8$: $0.94e^-$ per $Li_xMn_2O_4$ unit with FE of 0.92 at 0.53 C rate has been

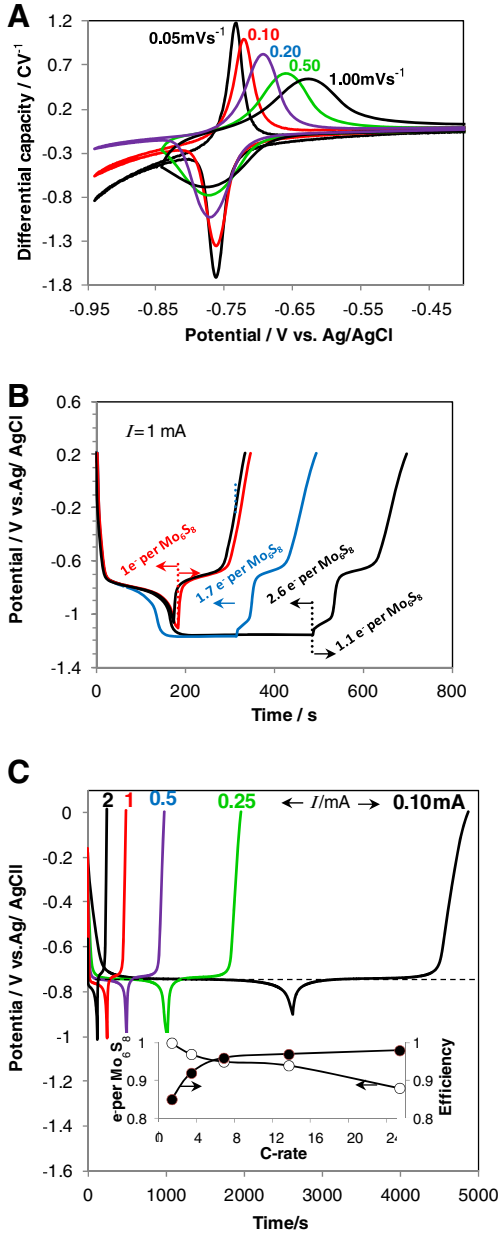


**Fig. 1** Cyclic voltammograms (**a**) and the related galvanostatic charge/discharge curves (**b**) for 1.6 mg $Mo_6S_8$ electrode. The charge was performed to different potentials (in the range from −1.06 to −1.16 V vs. Ag/AgCl) for different periods of time. The numbers of electrons per $Mo_6S_8$ unit calculated from the amount of the charge passed and the electrode mass are indicated in **b**. **c** Galvanostatic charge/discharge curves of 2.25 mg $Mo_6S_8$ electrode (current values are indicated). *Inset* in this panel shows the utilized capacity of the $Mo_6S_8$ electrode in terms of $e^-$ per $Mo_6S_8$ unit (*left*) and the Faradaic efficiency (*right*) as a function of the applied current, expressed in terms of C-rates. The *broken line* is a guideline to emphasize extreme flatness of the charge/discharge plateau. Solution composition, 2 M $Li_2SO_4$

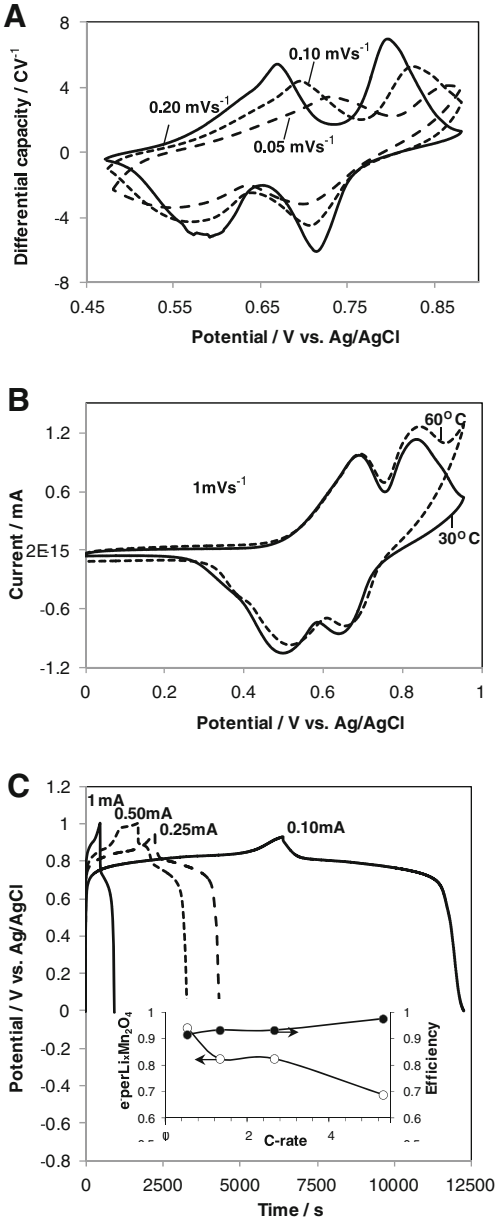


**Fig. 2** Cyclic voltammograms and the related galvanostatic curves measured with 1.27 mg $LiMn_2O_4$ electrode in a flooded cell with 2 M $Li_2SO_4$ solution (**a** and **c**, respectively). Scan rates and the values of the current applied are indicated. *Inset* in **c** shows the utilized capacity of the electrode in terms of $e^-$ per $Li_xMn_2O_4$ (*left*) and the Faradaic efficiency (*right*) as a function of the applied current presented in terms of C-rates. CVs shown in **b** were measured with 0.96 mg $Li_xMn_2O_4$ in a Hohsen-type cell with high electrode to solution mass ratio at 30 and 60 °C as indicated. The effect of the parasitic anodic reactions at the elevated temperature is clearly seen close to the anodic cut-off potential

reached (panel c). This electrode is, however, not as fast as $Mo_6S_8$: only $0.68e^-$ per $Li_xMn_2O_4$ unit has been reached with FE of 0.98 at the fastest rate applied (5.32 C).

Despite the different rate capabilities of $Mo_6S_8$ and $Li_xMn_2O_4$, and taking into account that these two electrodes have most negative and most positive redox potentials, respectively, ever known for aqueous solutions, we assembled a full cell taking the cathode in 50 % excess with

respect to the anode (to compensate the difference in their rate capabilities). Since the anode has a single voltage plateau in the chosen potential window, whereas the cathode possesses two plateaus, the depth of charge of the cathode can be controlled visually (in a qualitative manner), in addition to the accurate calculation of the stoichiometry of the Li-ion insertion–deinsertion process. Figure 3a shows the rate capability test of the full cell cycled to cut-off potential of 1.57 V. A single, very flat voltage plateau is indeed observed presumably due to coupling of the single $Mo_6S_8$ plateau with the first (lower in potential) plateau of $Li_xMn_2O_4$. In fact, when the cut-off potential was increased to 1.7 V (see Fig. 3b), the two charge–discharge plateaus became visible at moderate charging rates. Since $Li_xMn_2O_4$ was taken in excess with respect to the anode, the above result confirms our expectation that the transfer of $Li^+$ ions from the slower $Li_xMn_2O_4$ cathode to a faster $Mo_6S_8$ anode is feasible at the expense of the practical capacity delivered by the cathode. Plots of the depth of charge and the FE as a function of charging rate (calculated for the anode, limiting the capacity, see inset in Fig. 3b) even for the present non-optimized cell show a promising result: at high 13.7 C rate, the stoichiometry attained is $0.61e^-$ per $Mo_6S_8$ unit with FE of 0.98 and $0.91e^-$ per $Mo_6S_8$ unit with FE of 0.82 at slow 1.37 C rate. Continuous galvanostatic cycling test (100 cycles) at 70 % depth of $Mo_6S_8$ charge revealed that the capacity was unchanged with some modifications of the voltage profile probably due to a gradually increasing resistance of the cell (Fig. 3c).

Realizing that the major reason of the above increase in the cell resistance may relate with an insufficiently high rate capability of the cathode, and that this complication may be soon overcome in view of a rapid progress in the batteries' materials, we looked into the problem of the increase of the $Li_xMo_6S_8$ anode capacity by decreasing the electrode potential, provoking thus a strong interference of Li-ion insertion process with a parasitic reaction of electroreduction of water. First CV tests (inevitably performed at a high rate, here, 20 $mVs^{-1}$) revealed three distinct stoichiometries: $Li_1Mo_6S_8$, $Li_3Mo_6S_8$, and $Li_4Mo_6S_8$ (the latter heavily overlapping with the parasitic process of electroreduction of water) strikingly similar to that known for the $Mo_6S_8$ Chevrel phase in aprotic electrolyte solution with much higher electrochemical stability window (see Fig. 4a in comparison with the qualitatively similar CVs obtained for the $Mo_6S_8$ in propylene carbonate-based solutions, shown in Fig. 5). The CV shown in Fig. 5 together with the stoichiometry attained practically coincides with that obtained by slow galvanostatic charging of $Mo_6S_8$ in a similar propylene carbonate-based solution [14]. There is almost a triple increase of the charge capacity retrieved when the cut-off potential is decreasing from −1.17 to −1.64 V, i.e. changing the stoichiometry from $Li_1Mo_6S_8$ to $Li_3Mo_6S_8$.

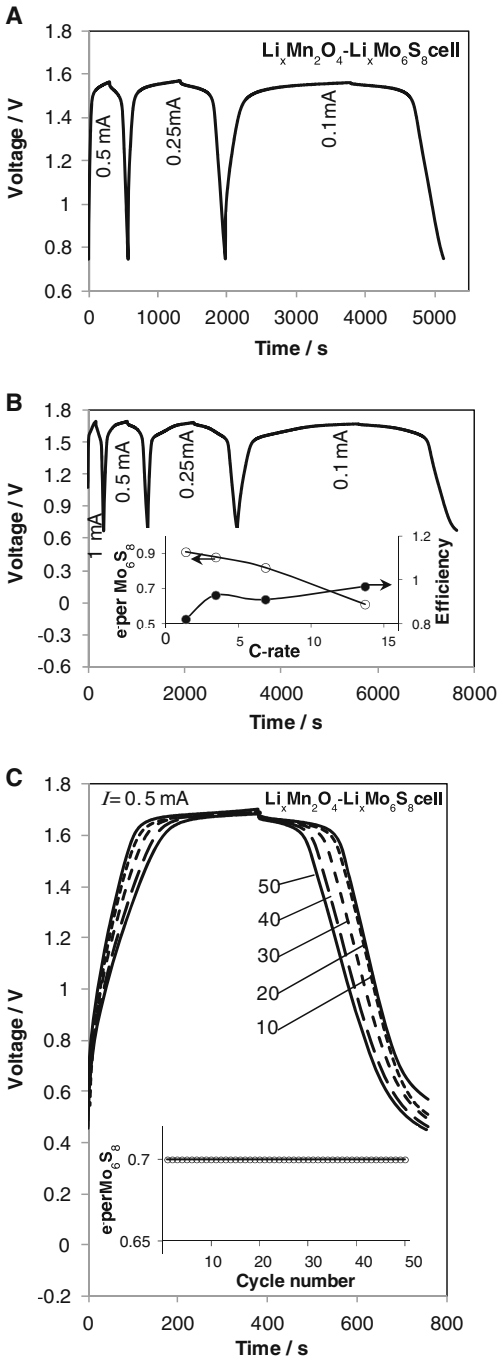


**Fig. 3** Charge/discharge curves of $Li_xMn_2O_4/Li_xMo_6O_8$ cell (2.35 mg of $Mo_6O_8$ anode and 0.75 mg of $Li_xMn_2O_4$ cathode (50 % excess with respect to the anode)) measured at different currents up to the cut-off voltage of 1.57 V (**a**) and to a higher cut-off voltage of 1.7 V (**b**). *Inset* in panel **b** shows the utilized capacity of the electrode in terms of $e^-$ per $Mo_6S_8$ (*left*) and the Faradaic efficiency (*right*) as a function of the applied currents presented in terms of C-rates. **c** Charge/discharge curves of the same cell for consecutive 50 cycles using applied current 0.5 mA and 70 % utilization of the $Mo_6S_8$ anode capacity. The voltage profiles for 10th, 20th, 30th, 40th, and 50th cycles are indicated. *Inset* in this panel demonstrates constant anode's stoichiometry of 0.7 $e^-$ per $Mo_6S_8$ under 13.7 C rate (0.5 mA)

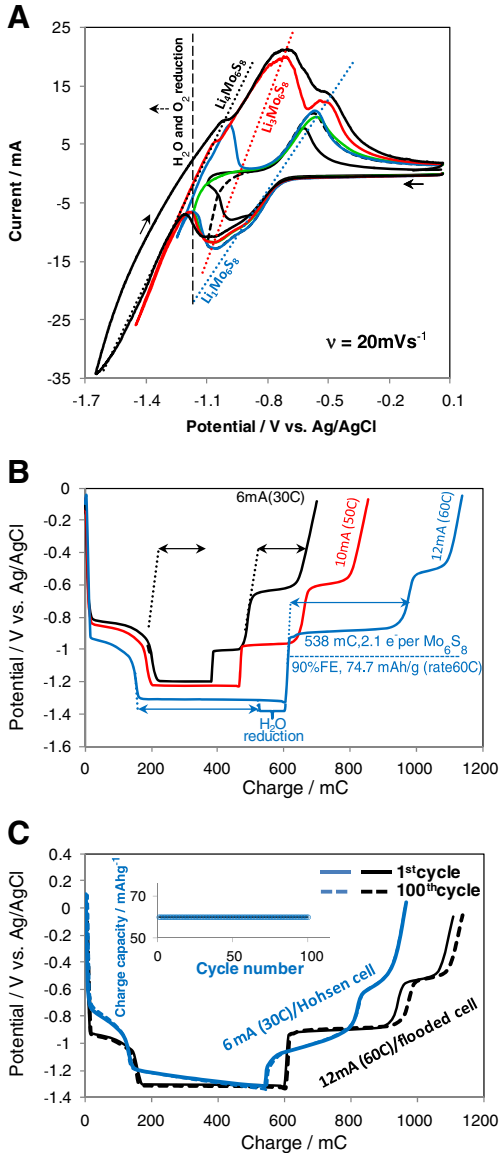


**Fig. 4** **a** Cyclic voltammograms which probe the unstable stoichiometries of the $Li_xMo_6S_8$, $x>1$ (2.25 mg) in 2 M $Li_2SO_4$ aqueous solution. The *dotted lines* mark the thermodynamically stable range of $Mo_6S_8/Li_1Mo_6S_8$ redox transition, quasi-stable stable $Li_1Mo_6S_8/Li_3Mo_6S_8$, and unstable $Li_3Mo_6S_8/L_4Mo_6S_8$ redox transitions (the parasitic reactions due to $H_2O$ electroreduction). Scan rate 20 $mVs^{-1}$. **b**, **c** Galvanostatic charge/discharge curves of $Li_xMo_6S_8$/activated carbon half-cell (2.0 mg of $Mo_6S_8$). In **b**, the curves relate to a flooded (volume 4 ml) well-deaerated cell with sat. Ag/AgCl reference electrode. Different polarization currents shifting the potential down to −1.3 V for the different periods of time were applied in order to explore both single-electron and two-electron reduction of $Mo_6S_8$ optimizing the delivered practical capacity and the Faradaic efficiency (*FE*) beyond the thermodynamically limited boundary of water reduction as indicated. **c** The subsequent galvanostatic cycling of the same $Mo_6S_8$ electrode both in flooded cell (the *black curves*) and in a Hohsen-type semi-starved cell (the *blue curves*) at 60 and 30 C-rates, respectively, for the 1st and 100th cycles (the *solid* and *dashed lines*, as indicated). *Inset* in **c** shows the delivered specific capacity during first 100 cycles for the semi-starved cell

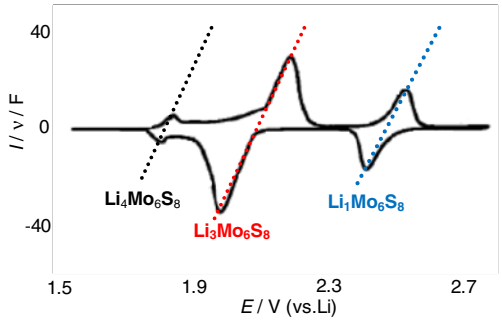


**Fig. 5** Differential capacity curves for the $Mo_6S_8$ electrode obtained from the related CV in 1 M $LiClO_4$/propylene carbonate solution at 25 $\mu Vs^{-1}$. The stoichiometry attained at different potential ranges is indicated

Figure 4b, c presents results of the galvanostatic tests of $Mo_6S_8$ in half cells (both in flooded and semi-starved Hohsen-type cells). The results for three different currents with different cut-off potentials and polarization times are shown in Fig. 4b. Two black curves shown in this figure prove that the amount of charge retrieved during the $Li_x$-$Mo_6S_8$ electrode delithiation is independent of the cut-off potential even when this potential reaches the lower $Li_x$-$Mo_6S_8$ plateau with practically 1.0 FE. The percent of the charge retrieval is much less along the lower voltage plateau depending both on the current value and the residence time along this plateau: an increase in both quantities affects the FE in opposite directions. By optimizing these two parameters, we reached an amazingly high capacity of the $Mo_6S_8$ anode (74.7 $mAhg^{-1}$ corresponding to $2.1e^-$ per $Mo_6S_8$ unit, see Fig. 4b) with excellent FE of 90 % at 60 C rate. Figure 4b visualizes the involvement of water electroreduction process in the entire charge process which is estimated to be 10 %.

One of the major concerns related to the above result is whether the $Mo_6S_8$ electrode is able to retain this high capacity during its long-term cycling. The electrode was thus cycled 100 times at the same rate in flooded cell geometry, and after completing the galvanostatic test, it was placed into a semi-starved Hohsen-type cell with a piece of K2000 carbon as the counter-electrode. Solid and dashed black curves in Fig. 4c show that the capacity in the flooded cell is even slightly increased from 1st to 100th cycle without any substantial change in the voltage profile. Since we used the same electrode for another 100 cycles in the Hohsen cell, the voltage profile in this cell shown by the blue curves in Fig. 4c, especially the sloping voltage plateaus, is evident of a larger Ohmic resistance in this cell compared to that in the flooded cell (for this reason, the charging current was chosen to be half of that for the flooded cell). No change in the voltage profile has been detected over 100 cycles: the cell was successfully cycled, delivering 60 $mAhg^{-1}$ specific capacities. Assuming that an ultrafast cathode with a specific capacity around that of

$Li_xMn_2O_4$ (120 $mAhg^{-1}$) will be developed as a couple to the ultrafast $Mo_6S_8$ anode with similar redox potential of 0.75 V, this will translate into 40 $mAhg^{-1}$ of the specific capacity (based on the balanced mass of both electrodes) leading to specific energy of the cell $40 \times 1.85 = 74$ $Whkg^{-1}$, which is by 50 % higher than that reported recently for the aqueous $Li_xTi_2(PO_4)_3/Li_xFePO_4$ battery [5].

## Conclusion

We found evidence that the $Mo_6S_8$ Chevrel phase compound is an ultrafast anode, which can be coupled with a moderately fast $Li_xMn_2O_4$ cathode in an aqueous Li-ion battery with the cell voltage as high as 1.5 V ($1e^-$ transfer in $Mo_6S_8$ at −0.75 V). By using extraordinary fast rate of Li-ion insertion into $Mo_6S_8$, we show that it is *kinetically* feasible to reach the second $2e^-$ reduction of $Mo_6S_8$ (redox potential −1.1 V), beyond the thermodynamic (i.e., close to equilibrium) limit of stability of aqueous solutions, effectively discriminating the reaction of electroreduction of water at high charging–discharging rate. This discrimination is due to the fact that the parasitic reaction of electrochemical decomposition of water is a stationary process, only slightly dependent on the charging rates, whereas Li insertion reaction is a typical non-stationary process with the current in the CVs curves proportional to the scan rate. During slow galvanostatic charging, too small applied currents may support the parasitic reactions preventing the cell from reaching the pre-defined cut-off potentials for the Li insertion process, thus decreasing the FE of the insertion process. In contrast, when large applied currents are applied, the cut-off potential of Li insertion/deinsertion reaction is reached in a short period of time, limiting the involvement of the parasitic reactions and hence increasing formally the FE. The high voltage aqueous Li-ion cell chosen in this study raises an important problem related to the current R&D work in the entire field of AqLiB, namely, the possibility of suppression of the parasitic reactions accompanying charging processes in these batteries. A positive effect of removal of oxygen has been repeatedly reported [5–7] and has been also confirmed in this work. The increase in the solution pH was recommended in refs. [5, 15]. We have found that $Mo_6S_8$ electrode shows a rather poor performance at pH=13, thus the effect of pH is electrode-dependent. Importantly, a positive effect of the increase in the concentration of $Li_2SO_4$ or $LiNO_3$ on cycling performance of AqLiB has been noted by a number of researchers, which in our opinion, is due to a decrease of the activity of bulk water, reducing its parasitic reactions. The field of AqLiB is too young, and only a small part of the vast arsenal of knowledge accumulated by the electrochemistry of aqueous solutions has been used by the researchers to tackle the problem of fast self-discharge of the intercalation electrodes in AqLiB. Further research in the following directions could presumably solve the problem of fast self-discharge: (a) a careful purification of the salts (high concentration is used!) and water for preparation of the solutions; (b) the use of mixed organic solvent–water mixtures with the purpose to decrease water activity, and (c) surface-active additives, possibly, of hydrophobic character to inhibit surface activity of water (however, a compromise with a full impregnation of the active electrode mass by solution should be maintained); and (d) studies of the ion insertion host/solution interface and of the ion's transfer through the interface; surface and structure analysis of the electrodes (both ex situ and in situ) may also appear to be useful in this respect. Once the problem of self-discharge is solved, the development of intelligent aqueous Li-ion batteries supplied with precise voltage control allowing for a flexible switching between high and low operating voltage mode could enormously improve the performance of AqLiB.

**Acknowledgments** We are thankful to Dr. M. Potel and Prof. M. Guilloux Viry (Unité des Sciences Chimiques de Rennes, Rennes University) for providing with the Chevrel phase powders.

## References

1. Ozawa K (ed) (2009) Lithium ion rechargeable batteries. Wiley, Weinheim
2. Li W, Dahn J, Wainwright D (1994) Science 264:1115
3. Li W, McKinnon WR, Dahn JR (1994) J Electrochem Soc 141:2310
4. Li W, Dahn J (1995) J Electrochem Soc 142:1742
5. Luo JY, Cui WJ, He P, Xia YY (2010) Nat Chem 2:760
6. Luo JY, Xia YY (2007) Adv Funct Mater 17:3877
7. Wang YG, Luo JY, Wang CX, Xia YY (2006) J Electrochem Soc 153:A1425
8. Wessells C, Ruff R, Huggins RA, Cui Y (2010) Electrochem Solid State Lett 13:A59
9. Levi MD, Lancry E, Gizbar H, Lu Z, Levi E, Gofer Y, Aurbach D (2004) J Electrochem Soc 151:A1044
10. Gocke E, Schramm W, Dolscheid P, Schollhorn R (1987) J Solid State Chem 70:71
11. Kaidi Z, Boulanger C, Lecuire JM, Lemke N, Guilloux-Viry M, Perrin A (1999) Solid State Sci 1:623
12. Seghir S, Boulanger C, Diliberto S, Lecuire JM, Potel M, Merdrignac-Conanec O (2008) Electrochem Commun 10:1505
13. Seghir S, Boulanger C, Diliberto S, Potel M, Lecuire JM (2010) Electrochim Acta 55:1097
14. Gocke E, Schollhorn R, Aselmann G, Muller-Warmuth W (1987) Inorg Chem 26:1805
15. Zhang M, Dahn JR (1996) J Electrochem Soc 143:2730